Fachtagung "Lasermethoden in der Strömungsmesstechnik"
6.–8. September 2011, Ilmenau

Parameter Sensitivity of Optical Flow Applied to PIV Images

Einfluss von Parametern bei der Anwendung des Optischen Flusses auf PIV Bilder

R. Kapulla[*], P. Hoang[*], R. Szijarto[**], J. Fokken[*]
[*]Labor für Thermohydraulik (LTH), Paul Scherrer Institut, 5232 Villigen, Schweiz
[**]Institute of Nuclear Techniques, Budapest University of Technology and Economics, Műegyetem rkp. 3-9. H-1111 Budapest, Hungary

Abstract

To overcome some limitations of the classical cross correlation based PIV analysis, such as the spatial resolution being determined by the final interrogation window size, researchers have been exploring the Optical Flow (OF) method. This technique relies on the apparent movement of the recorded brightness patterns caused by illuminated particles in a flow. The OF method implemented for the present study is based on a variational flow estimate making use of an additional smoothness constraint. In the implementation of the OF method the a priori numerical values of the (i) smoothness weight factor and (ii) the influence of preprocessing filters homogenizing local intensity variations throughout the recorded images are not well known. An assessment of these parameters requires knowledge of the underlying velocity field. Consequently, two synthetically generated images pair sets are used to have a complete analytical solution available for comparison. It will be shown that a distinct optimum for the smoothness weight factor can be found for which the calculated error measures are minimized and that the intensity normalization prior to the OF application is of utmost importance.

1 Introduction

Since the classical cross correlation based PIV analysis suffers from some fundamental limitations such as (i) the spatial resolution of the estimated velocity field being determined and limited by the final interrogation window size, (ii) the relative movement of the particles in an interrogation window with respect to each other are assumed to be negligible, (iii) the motion estimate being carried out regardless of the spatial context [10] and (iv) the sensitivity of the cross-correlation based PIV method to optical distortions subject to the experimental setup, researchers have been exploring alternative analysis methods. One such method is the Optical Flow method (OF).

In the implementation of the OF method the a priori numerical values of certain user adjustable parameters are not known. The most prominent among these parameters is the smoothness weight factor which relates the error introduced by the smoothness constraint with the error introduced by non ideal recording conditions resulting in local intensity variations. Other parameters include the number of pyramid and scale levels and the use of preprocessing filters homogenizing the intensity variations throughout the recorded images. The well-founded selection of these parameters, however, require prior knowledge of the underlying velocity field. Consequently, two data sets are examined. In each data set, image pairs are synthetically generated so as to each have a complete analytical solution available. One series is comprised of images published by the Visual Society of Japan [9], whereas the other series is based on Large-Eddy-Simulations (LES) performed for isokinetic mixing experiments in a square channel. The objective of this paper is to systematically examine the influence of the (a) smoothness weight factor and

of the (b) preprocessing filters normalizing local intensity variations common for PIV recordings on the error budget.

In the next section, we give a brief introduction into the OF method implemented. This is followed by a description of the image sets used (sect. 3) and an explanation of the intensity normalization applied (sect. 4). After the introduction of the error measures used (sect. 5) we discuss the benchmark calculations on the basis of the two image sets and bring the results in perspective with the classical PIV cross correlation approach (sect. 6). We conclude in sect. 7 with possible improvements of the OF approach.

2 Optical Flow Principles

The method considered here is the Optical Flow (OF) method as reported in [4]. This technique relies on the apparent movement of the recorded brightness patterns caused by illuminated particles in a flow. Let $I(i, j, t)$ denote the gray value at location (i, j) and time t in the image plane with dimensions mxn, $i \in [1\ m]$ and $j \in [1\ n]$. If the brightness of a particular point remains constant when 'moved' by the local apparent velocity components $u = di/dt$ and $v = dj/dt$ during a small time instance dt to another location $(i + di, j + dj)$ between the recording of image pairs, i. e. $I(i, j, t) = I(i + di, j + dj, t + dt)$, the substantial derivative for the intensity – the brightness transport equation – can be written as:

$$\frac{DI}{Dt} = 0 = \frac{\partial I}{\partial i}\frac{di}{dt} + \frac{\partial I}{\partial j}\frac{dj}{dt} + \frac{\partial I}{\partial t} = I_i u + I_j v + I_t \tag{1}$$

Since the velocity vector has two components (u, v), whereas the change in brightness at a point provides only one constraint, an additional condition is necessary to solve eq. (1). Based on the assumption that neighboring points have similar velocities, a smoothness constraint is introduced ([4] and [10]) such that the spatial velocity gradients

$$|\nabla u|^2 = \left(\frac{\partial u}{\partial i}\right)^2 + \left(\frac{\partial u}{\partial j}\right)^2 \text{ and } |\nabla v|^2 = \left(\frac{\partial v}{\partial i}\right)^2 + \left(\frac{\partial v}{\partial j}\right)^2 \tag{2}$$

will be minimized. For a real recording system the intensity does not remain constant and the conditions for the velocity field solving eq. (1), will be relaxed such that the problem posed is to minimize the sum

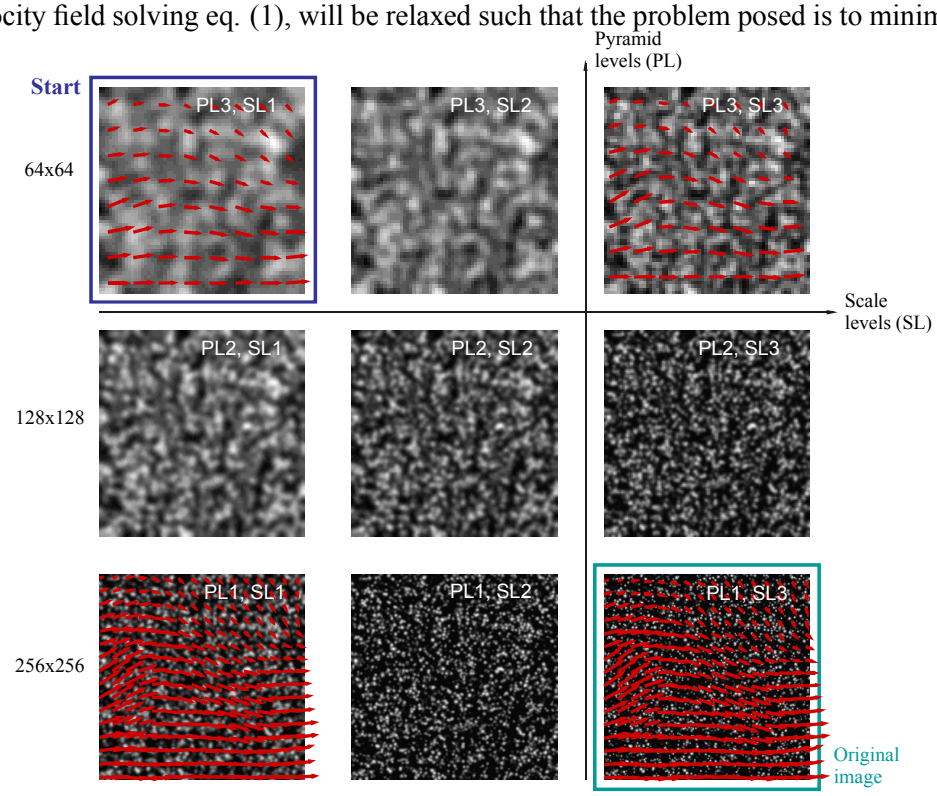

Figure 1: *Schematic of the OF method using three Gaussian pyramid levels (PL) and three scale levels (SL). The original image (PL1, SL3) has a resolution of 256x256.*

of errors for the brightness transport equation E_B and the departure from smoothness E_C^2, i.e.

$$E_B = I_i u + I_j v + I_t$$

$$E_C^2 = |\Delta u|^2 + |\Delta v|^2$$

which results in minimizing the total error E with the weighting factor α^2:

$$E = \int\int \left\{ E_B^2 + \alpha^2 E_C^2 \right\} didj \tag{3}$$

while finding a suitable velocity field. The OF method implemented for the present study is combined with a Gaussian pyramid level (PL) and an additional scale level (SL) representation of the images (Fig. 1) to overcome spatial aliasing issues as described in [10] and [6]. The Gaussian pyramid levels [5] are calculated starting with the original image by repeatedly downsampling , i.e. for each pyramid level the spatial resolution is reduced by a factor of two, Fig. 1. To avoid Moiré-effects (spatial aliasing) during the calculation of the PL, a spatial low-pass filter having a cut-off frequency of $\pi/2$ is applied each time in advance. On each PL additional SL are calculated again using Gaussian filters with cut-off frequencies linearly varied in the range $[\pi/2, \pi]$ over the SL. For a given PL, this results again in a coarse-to-fine image sequence. The initial velocity field estimate is then calculated with the OF method for the coarsest image pair PL3, SL1 and successively refined (PL3, SL1 →PL3, SL2→PL3, SL3) until the original image (PL1, SL3) is reached. The details of this process can be found in [10] and [6].

3 Images Used

The error budget evaluation was carried out on the basis of two synthetically generated image data sets. One data set comprises of PIV standard images made public by the Visual Society of Japan where the underlying flow field was calculated using LES [9]. These images are hereinafter abbreviated with VSJ. The parameters of these images can be found in Table 1 and the details of these images are thoroughly described in [9] and [10].

Image No -	Av. disp. [pixel]	Max disp. [pixel]	Av. out of plane vel. [pixel]	No. of particles -	Av. part diameter [pixel]	Std. dev. diameter [pixel]
01	7.4	15	0.017	4′000	5	1.4
02	**22.2**	**45**	**0.058**	4′000	5	1.4
03	**2.5**	**5**	**0.006**	4′000	5	1.4
04	7.4	15	0.017	**10′000**	5	1.4
05	7.4	15	0.017	**1′000**	5	1.4
06	7.4	15	0.017	4′000	5	**0.0**
07	7.4	15	0.017	4′000	**10**	4.0
08	7.4	15	**0.170**	4′000	5	1.4

Table 1: *Characteristic parameters for the generation of the synthetic VSJ images. Variations from the default settings are marked in bold. The Table was taken from* [10]

An example image (VSJ_01), the flow field and the upper left corner of the entire image set can be found in Fig. 2. Since the VSJ images experience a lack of completeness with respect to for example the grad fineness of the time difference Δt between image pairs expressed as the average displacement (Av. disp.) in Table 1, it was decided that a second set of synthetic images should be generated based on LES calculations. These images would simulate image pairs created for isokinetic conditions in a square channel for a mixing experiment [2], [3] and [6], where OF should be applied. In these experiments two streams of water with equal or different density initially separated by a splitter plate interact downstream from the tip of this plate. The second set of images was generated using the EUROPIV Synthetic Image Generator [8].

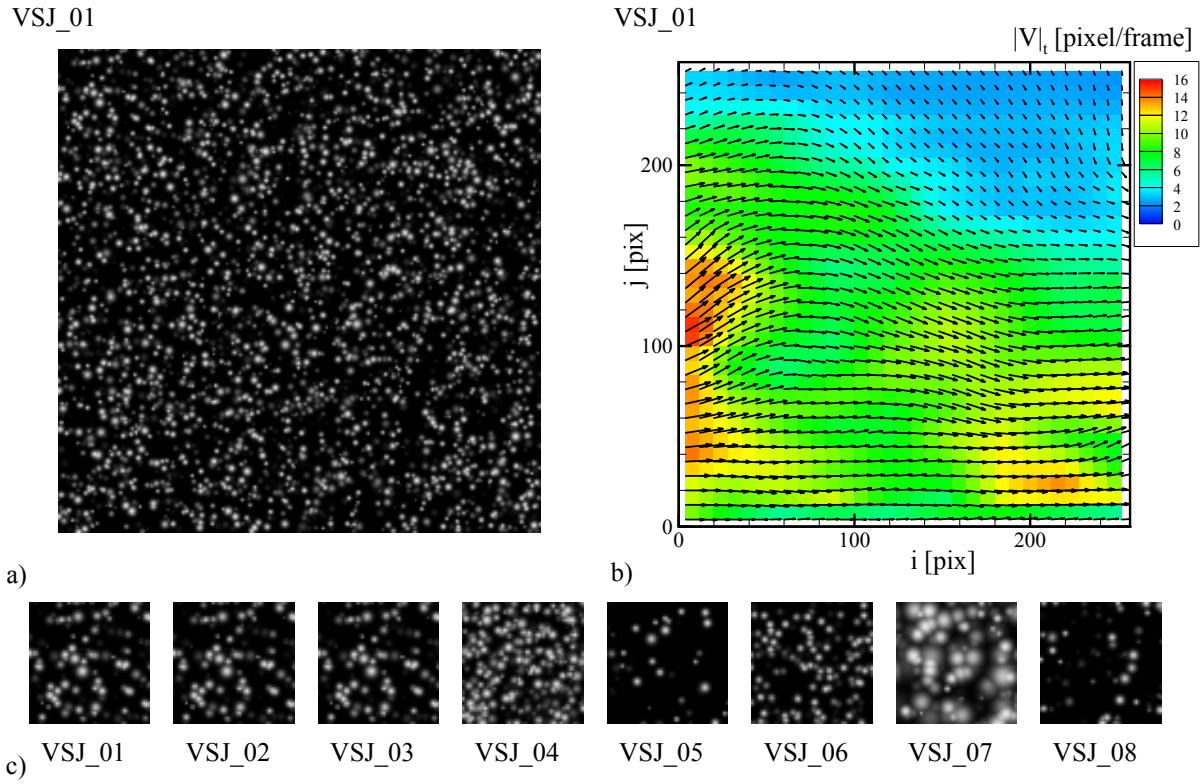

Figure 2: *Example of the synthetically generated VSJ standard image 01 a), the underlying velocity field b) and a 50x50 pixel^2 region of the upper left corner of VSJ images 01 through 08.*

Overall, we generated 20 different image pairs (GEM_09 through GEM_28) and the main characteristics of these images can be found in Table 2. Sample image (GEM_12), the flow field and an extract of the various image distortions introduced can be found in Fig. 3. The details of the flow field in terms of the velocity components u and v are presented in Fig. 6.

Image No -	Av. disp. [pixel]	Max disp. [pixel]	Av. out of plane vel. [pixel]	No. of particles -	Av. part diameter [pixel]	Std diameter [pixel]
09	2.6	4.0	0.0485	6′000	2	0
10	5.3	7.2	0.0970	6′000	2	0
11	7.9	10.1	0.1455	6′000	2	0
12	10.6	14.3	0.1940	6′000	2	0
13	13.2	17.3	0.2425	6′000	2	0
14	15.9	20.1	0.2910	6′000	2	0
15	21.2	27.1	0.3880	6′000	2	0
16 - 28	10.6	14.3	0.1940	6′000	2	0

Table 2: *Characteristic parameters for the generation of the synthetic GEM images.*

For all of the images, the generation parameters, (i.e. number of particles, particle mean diameter etc.) were kept constant. For the first subset of images (GEM_09 through GEM_15), we systematically varied the time difference Δt between image pairs, resulting in mean pixel displacements ranging from 2.5 to 21.2 pixels. Image GEM_12, with an average displacement of 10.6 pixel, is regarded as the base image to which different types of distortions were added. For a second subset (GEM_16 through GEM_19), we degraded the images by the superposition of 10, 20, 40 and 60 % Gaussian noise, Fig. 3 c) and in a third

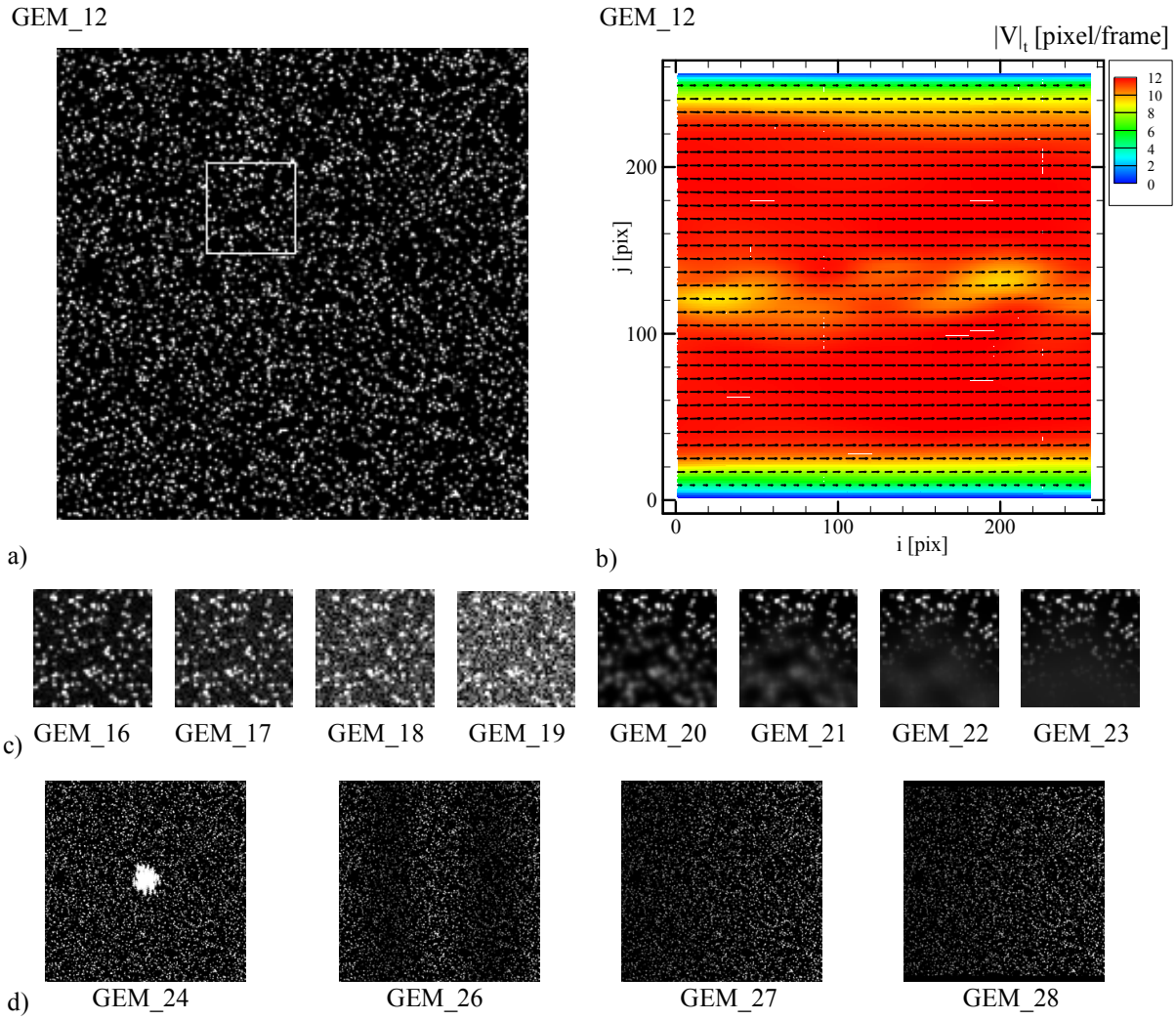

Figure 3: *Example of the synthetically generated GEM image 12 a), the underlying velocity field b) and a 50x50 pixel^2 region extracted from images 16 through 19 with increasing noise content as well as images 12 through 23 where the middle region was blurred c) and images 24 through 28 with local intensity changes common in PIV image sequences .*

subset (GEM_20 through GEM_23) we blurred the central region of the flow using different Gaussian filters to mimic optical distortions caused by refractive index variations between the upper and the lower part of the flow [6]. A more detailed image of this blurring is pictured in the upper row of Fig. 4.

Finally, in a fourth sub set of images (GEM_24 through GEM_28), we introduced local intensity variations common in PIV recordings. Image GEM_24 contains a large bright spot, image GEM_26 contains a double left-right brightness undulation, GEM_27 contains a linear left-right intensity variation from dark to bright and finally image GEM_28 contains a left-right intensity variation with additional black borders at the top and bottom, simulating the masking of test section components.

4 Intensity Normalization

In contrast to the correlation based PIV technique which relies to a lesser extent on the brightness of the particle patterns, the OF method might experience considerable distortions arising from either changes in refractive index between the upper and lower stream or by local intensity variations quite common in PIV image sequences, Fig. 4. The influence of these distortions on the OF result will be shown in a subsequent section

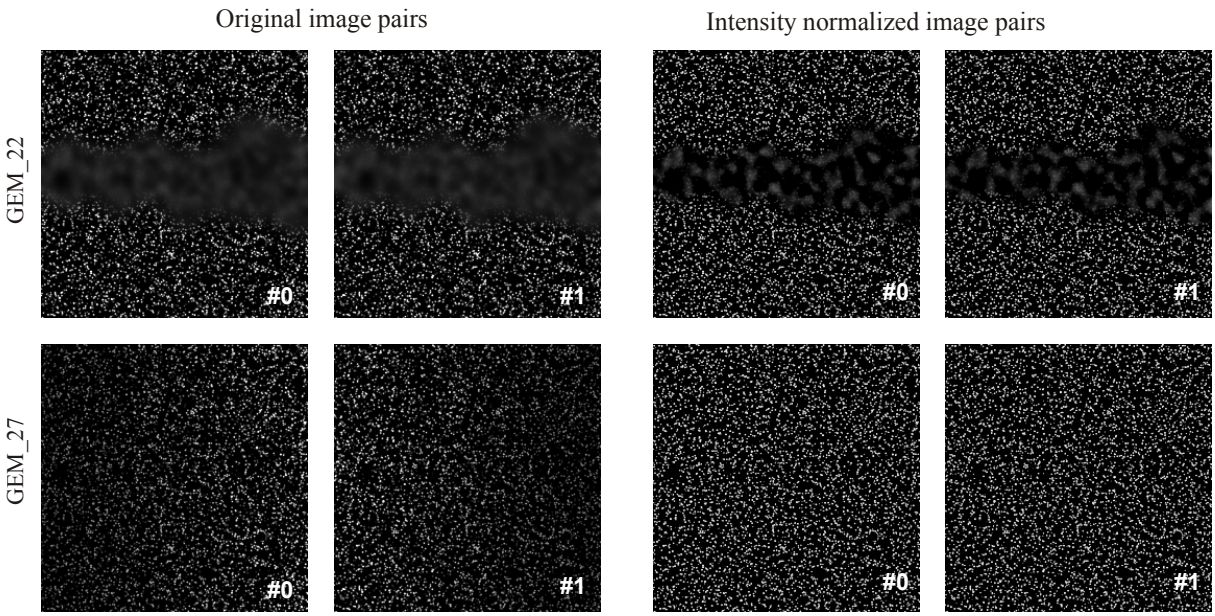

Figure 4: *Result of the intensity normalization applied to images of the second batch of synthetic images with the refractive index type of distortion in the developing zone of the mixing layer (GEM_22) and a local brightness variation from left to right and right to left (GEM_27).*

To cope with the brightness variations, the intensity of the images were normalized prior to the application of the OF method with a digital filter sequence inspired by a method and filters described in [7]. The details of the algorithm can be found in the appendix and the effect of this method is pictured in Fig. 4.

5 Error Quantities

We computed the displacement and the angular errors as quantitative error measures. In general, the two dimensional velocity vector $\mathbf{V}$ is denoted with $\mathbf{V} = \{u(i,j), v(i,j)\}$ and the magnitude of $\mathbf{V}$ was calculated accordingly $|\mathbf{V}(i,j)| = \sqrt{u^2+v^2}$. The indices '$e$' and '$t$' depict the **e**stimated values (according to either the optical flow or the PIV calculations) and the '**t**rue' value which is provided by LES calculations, respectively. To condense the error budget into a single numerical value, the *average absolute magnitude error* $|\mathbf{V}|_{a,m}$ is calculated with:

$$|V|_{a,m} = \frac{1}{m \cdot n} \sum_i \sum_j \left(||\mathbf{V}_e(i,j)| - |\mathbf{V}_t(i,j)|| \right) \qquad [pixel/frame] \tag{4}$$

and the *average relative magnitude error* $|\mathbf{V}|_{r,m}$ accordingly:

$$|V|_{r,m} = \frac{|V|_{a,m}}{\frac{1}{m \cdot n} \sum_i \sum_j \left(|\mathbf{V}_t(i,j)| \right)} \cdot 100 \qquad [\%] \tag{5}$$

to account for the different average pixel displacements in the VSJ image series (Table 1) according to the suggestion in [10]. Following a suggestion in [1] we additionally calculated the *average angular*

error:

$$\psi_{a,m} = \frac{1}{m \cdot n} \sum_i \sum_j \arccos \left\{ \frac{u_e u_t + v_e v_t}{|V_e(i,j)|\,|V_t(i,j)|} \right\}) \qquad [^\circ] \tag{6}$$

6 Results

For the OF code assessment, the VSJ images 01 through 08 were used to apply the OF method as well as the standard cross correlation based PIV method for comparison purposes. The PIV analysis was performed with DaVis 7.2.2.426 from LaVison using a multi pass approach with decreasing interrogation window sizes starting with 64x64 reduced down to 16x16 with 50 % overlap. Using an image size of 256x256, this results in a final velocity field on a grid of 32x32. Trying to mimic the OF conditions described in [10], we used 5 pyramid levels (PL) and 9 scale levels (SL). The smoothness parameter was set to $\alpha = 0.3$ which corresponds to $\alpha^2 = 0.09$, which is almost ten times larger than the corresponding value of $7 \cdot 10^{-3}$ reported in [10]. The cut-off frequency of the Gaussian filter was linearly varied over the SL in the range $[\pi/2\ \pi]$. Applying eq. (4) and eq. (5) to the PIV and OF velocity field results in an absolute and relative error measure for the entire field, Fig. 5.

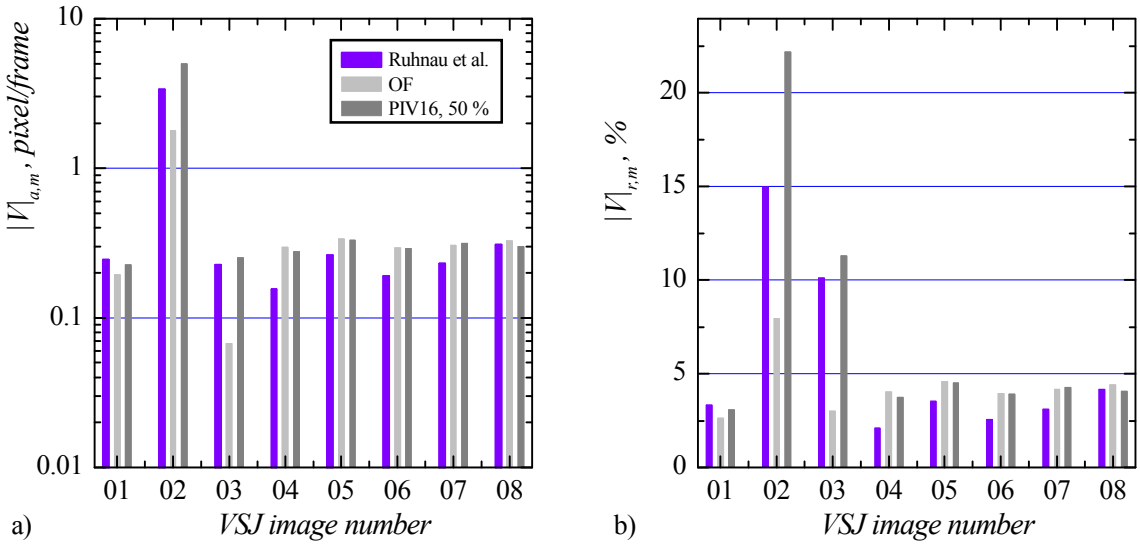

Figure 5: A*verage absolute magnitude error* $|V|_{a,m}$ *a) and average relative magnitude error* $|V|_{r,m}$ *b) for the VSJ images 01-08. Comparison of the results presented in* [10] *with own OF and PIV calculations.*

Overall, our OF results correspond very well with the OF results reported in [10]. There are some minor differences between our results and Ruhnau's such as the Ruhnau's method being consistently better in predicting the velocity field for images 03-08, while our calculations being better at predicting the velocity field for images 01-03. Additionally, the errors from our OF results and our PIV results are almost identical for images 04-08. Our OF method, however, decreased the absolute and relative error compared to PIV for images 01-03. It should be noted that even though the absolute error for VSJ image 03 is comparable to images 01 and 04-08, the reason its relative error so much higher than those images is because its average particle displacement is much lower, scaling its relative error upwards to reflect that.

The details of the original as well as the calculated flow field for the second set of GEM images can be found in Fig. 6 in terms of the velocity components u and v for image GEM_12. It should be noted that the entire velocity field is almost completely dominated by the velocity component u, the velocity ratio being $u/v \approx 120$. The OF calculations were performed with $\alpha^2 = 0.09$, $PL = 5$ and $SL = 9$. The overall agreement between the OF and LES results is good except for the lower left corner of the OF calculation and the ability of the OF method to resolve the steep gradients in the boundary layer close to the top and bottom walls, as also depicted by the extracted velocity profiles of the u component at

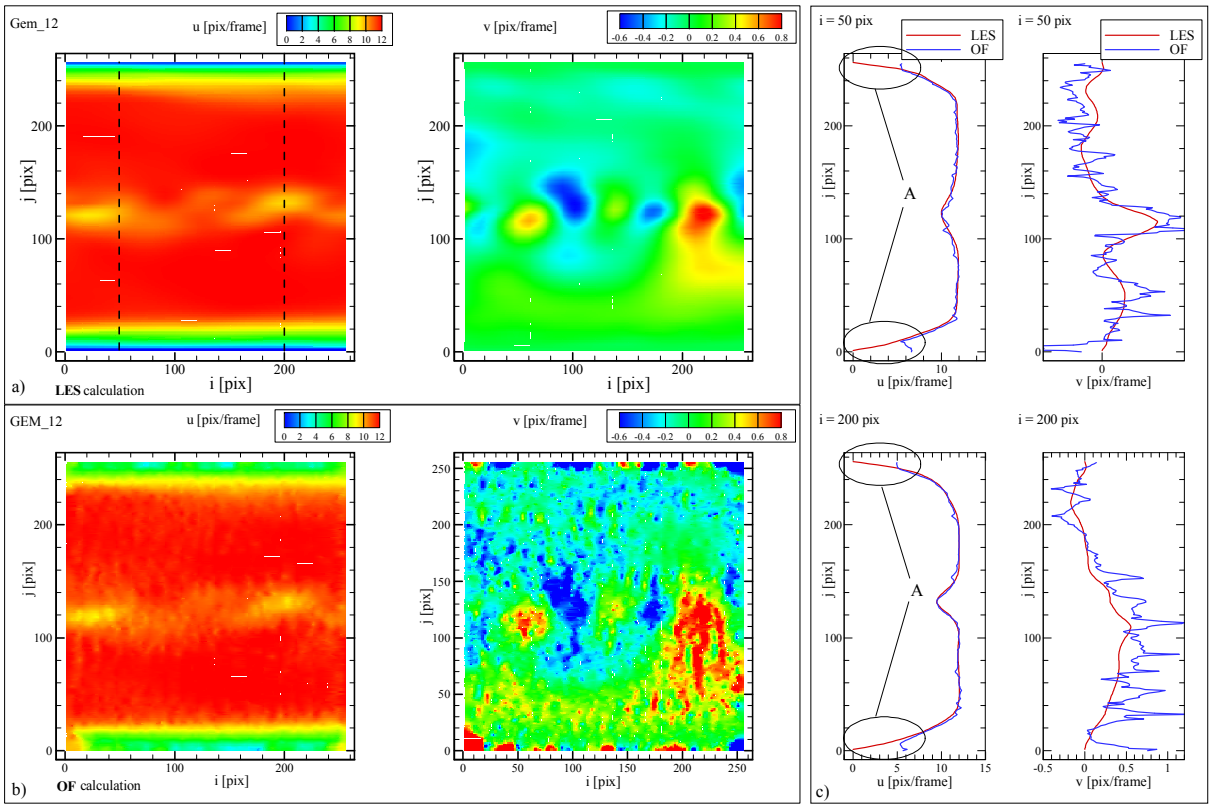

Figure 6: *Velocity components of the LES calculation for the mixing experiment in the test section GEMIX* [3] [2] *a), corresponding velocity field calculated with the OF method b) and comparison of LES and OF based velocity profiles at locations $x = 50$ and $x = 200$ pixel c).*

positions $i = 50$ and $i = 200$ pixel, Fig. 6 c) mark A.

For the present implementation of the code, α^2 is constant throughout the entire image; thus, neglecting local features of the flow such as strong velocity gradients in boundary layer zones. Consequently, the assessment of α^2 with respect to a global error measure such as $|V|_{a,m}$ is a 'good' value only on average. We believe that the introduction of a position dependent α^2, taking the velocity gradients from a previous calculation on a coarser scale or pyramid level into account, would considerably improve the results in regions characterized by strong velocity gradients. By lowering the numerical value of α^2 in such regions and therefore accordingly lowering the impact of the smoothness constraint in eq. (3), this would allow the solution to be less 'smooth', i.e. more steep. The overall shape of the crosswise velocity component v is sufficiently resolved by the OF method, but the results are very noisy with large local deviations from the LES result. This might suggest making α^2 not just position dependent, but also direction dependent. This is, however, subject of a refined discussion beyond the scope of this article.

To highlight the importance of image preprocessing prior to the application of the OF method, we present results for the average absolute magnitude error $|V|_{a,m}$ (eq. (4)) and the average angular error $\psi_{a,m}$ (eq. (6)) as a function of α^2 with the intensity normalization applied and not applied to the images (GEM_24 through GEM_28, Fig. 3) with initial strong intensity variations, Fig. 7. The results for image GEM_12 is given as a reference.

Applying the intensity normalization to the images GEM_24 through GEM_28 makes the shape of $|V|_{a,m} = f(\alpha^2)$ indistinguishably collapse onto the reference case (GEM_12) indicating (i) that the algorithm works properly , (ii) that it does not introduce artifacts and (iii) that the restored image quality competes with the original undistorted image. Increasing α^2 beginning at 10^{-4} makes $|V|_{a,m}$ decrease with a local minimum at $\alpha^2 \approx 0.09$ and an error budget of $|V|_{a,m} \approx 0.3$ pixel, the majority of which is caused by the faulty calculated velocities in the boundary layer, Fig. 6. Neglecting the velocity field boundaries in calculating the average absolute magnitude error results in $|V|_{a,m} \approx 0.1$ pixel, a typical error magnitude common for cross-correlation based PIV measurements. Increasing α^2 further, $|V|_{a,m}$ increases again and finally the error budget starts to level off. Interestingly, the angular error $\psi_{a,m}$ de-

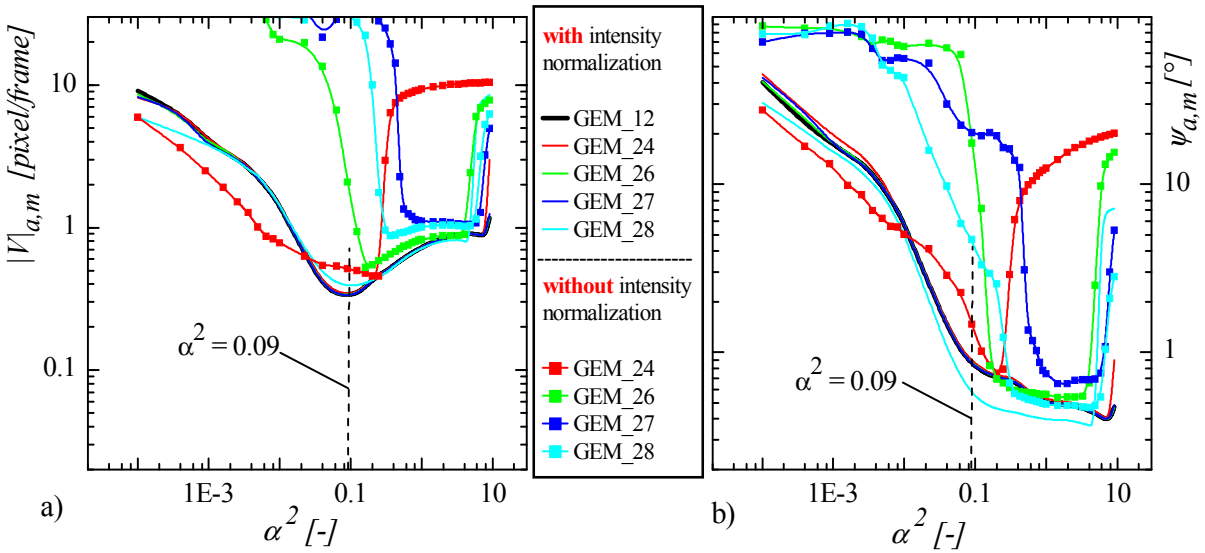

Figure 7: *Error measure $|V|_{a,m}$ and $\psi_{a,m}$ as a function of α^2 for image subset GEM_24 through GEM_28. For one calculation, the intensity normalization was applied to the images and for the other, it was not applied.*

creases further beyond the optimum of $\alpha^2 \approx 0.09$ determined from $|V|_{a,m}$ error budget which contrasts to the findings of similar calculations performed for the VSJ images discussed in the next section. This is probably attributed to the fact that the GEM images are somewhat biased by the lack of crosswise velocity content, (compare Fig. 2b to Fig. 3b). Not applying the intensity normalization results in $|V|_{a,m} = f(\alpha^2)$ shapes which considerably deviate from the reference case (GEM_12) indicating that the local image intensity variations considerably violate the constant intensity assumption used to derive the brightness transport equation (eq. (1)) and even the relaxed formulation of the problem (eq. (3)) for which the brightness changes are to be minimized.

In a similar manner as in Fig. 7, we present the results of the α^2 variation for the other batches of images in Fig. 9 in a compact graphical form to discuss the influence of Δt between image pairs (a to d), the noise level (e and f), the number of particle (g and h), the size of the particles (i and j) and the blur level (k and l), the lattermost mimicing possible optical distortions caused by refractive index variations. The reference images VSJ_01 and GEM_12 appear with an increased line thickness. The main difference between the aforementioned VSJ and GEM type of images is the shape of angular error budget $\psi_{a,m}$. Whereas $\psi_{a,m}$ decreases for the GEM type of images further beyond the optimum for $|V|_{a,m}$ with increasing α^2 we find the minimum in $\psi_{a,m}$ for the VSJ images coincide with the $|V|_{a,m}$ minimum. This can most likely be attributed to the lack of crosswise velocity content in the GEM images. Increasing α^2 puts more weight on the smoothness constraint resulting in flow fields with lower velocity gradients which preferentially optimizes the resulting velocity field in the u direction. From the results with the Δt variation (a to d) we can conclude on the basis of $|V|_{a,m} = f(\alpha^2)$ functions that the OF method preforms best with small Δt. This can be explained by making use of the correlation concept.

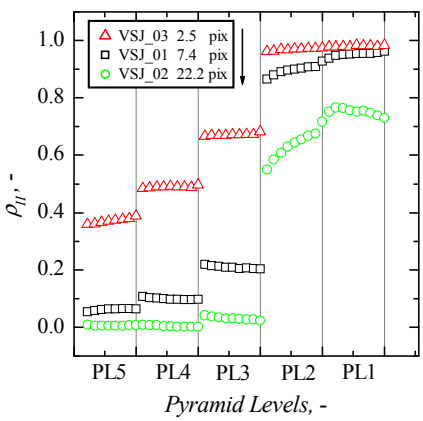

Figure 8: *Correlation strength ρ_{II} as a function of PL and SL.*

The minimizing velocity field $(u(i,j), v(i,j))$ (eq. (3)) maximizes the correlation $\rho_{II} = \sum I_1(i + u\Delta t, j + v\Delta t) \cdot I_0(i,j)$ between the two images, i.e. the intensity of the second image at locations $(i + u\Delta t, j + v\Delta t)$ is suppose to be similar to the location (i,j) of the first image since it was 'moved' from there. Underlying both image sets is a third, non-zero, out-of-plane velocity component. These out-of-plane velocities can on one hand move previously illuminated particles out of the 'light sheet' and on the other hand move new particles into the light sheet which were previously not visible.

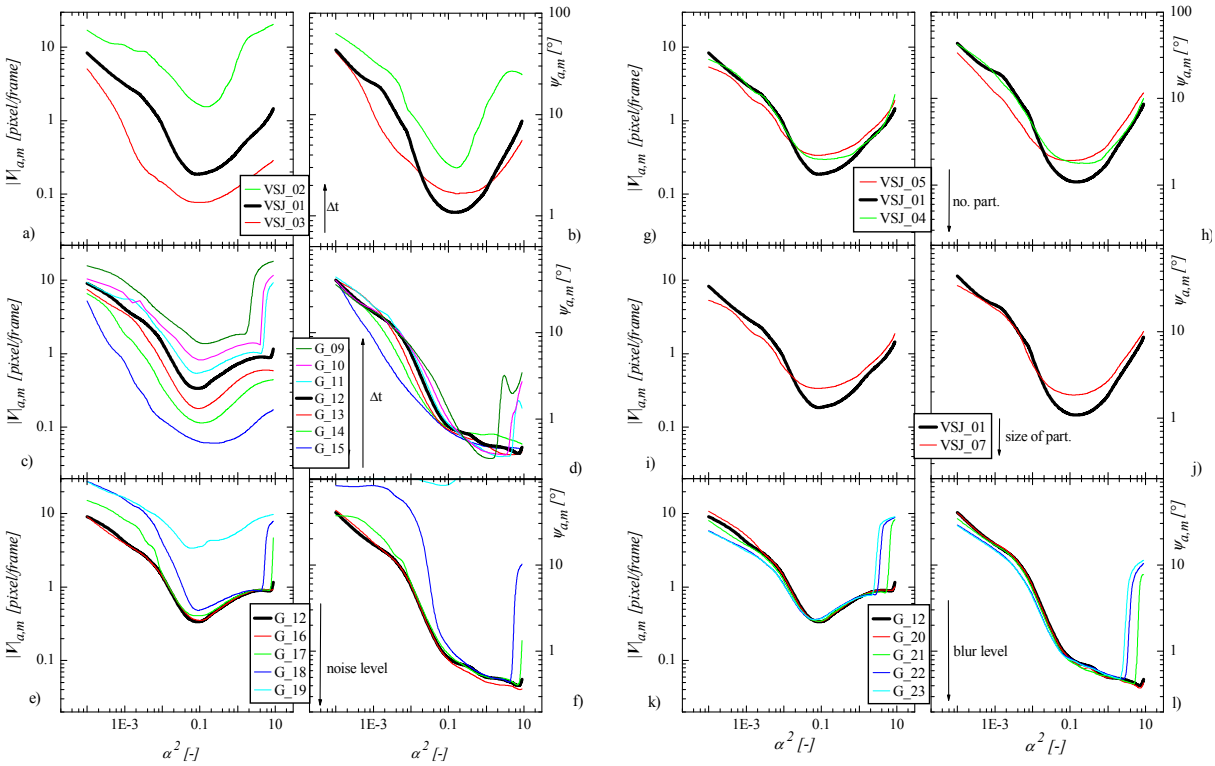

Figure 9: *Error measure $|V|_{a,m}$ and $\psi_{a,m}$ as a function of α^2 depicting the influence of Δt between image pairs (a to d), the number of particle (e and f), the size of the particles (g and f), the noise level (i and j) and the blur level (k and i).*

Consequently, even for a perfect velocity field, the correlation ρ_{II} will never reach unity. Increasing Δt increases the effect of the out-of-plane velocity, resulting in an overall de-correlation between the two images, which is, conversely reflected by the error budget $|V|_{a,m}$. This is shown in Fig. 8 where the velocity field on the different PL and SL was used to 'move' the particle intensities in the original sized images with subsequent ρ_{II} calculations. Besides using this method to track the progress and success of the OF method, the discussion of which is beyond the scope of this article, we find for the final correlation strength on PL1 the previously described dependence on image pair separation Δt.

For the noise level dependence of the results (e and f) as well as for the blur level (k and l) we find a remarkable resistance to noise up to levels of 40%. Even for the strongest blurring, the calculation remains unaffected, rendering the OF method suitable for even delicate recordings in demanding environments. The number of particles (g and h) seem less important than stated in [10] although the slightly better performance of VSJ_01 seems to indicate an optimum number density. A more detailed discussion must be postponed until more systematic calculations with varying particle numbers are available. Also the particle size seems to have a minor importance on the result. The remaining differences might be attributed to the fact, that VSJ images 01 to 03 and 04 to 08 seemed to be generated with different initial seed numbers for the initialization of the random number generator for the distribution the particles resulting in two distinct different batches of images as can be seen in Fig. 2 c) where the upper left corner of the VSJ images was enlarged. Therefore, the questions whether the differences just discussed are subject to physical properties such as particle size or the different particle distributions between batches must be left open.

7 Conclusions and Outlook

Parameter studies were performed with applying the optical flow technique to synthetically generated PIV-type images to assess the influence of the (i) preprocessing filters homogenizing different types of local intensity variations throughout the recorded images and (ii) the smoothness weighting factor on the error budget of the calculated velocity field. The error budget evaluation was carried out on the basis of two data sets. One data set comprises PIV standard images published through the Visual Society of

Japan (VSJ) and the other data set was generated in house (GEM). The overall error budget for the VSJ images was in good agreement with previously published results. However, the detailed discussion of the OF based velocity field for the GEM images revealed some weaknesses of the code when applied to strong velocity gradients, particularly in boundary layers. This flow situation acts counter towards to some extent the smoothness constraint (neighboring vectors have similar velocities) necessary to solve the brightness transport equation. To overcome this weakness, it is suggested for future applications to introduce a position and possibly also direction dependent smoothness parameter α^2 weighing the smoothness constraint according to the velocity gradients. The systematic variation of α^2 revealed the importance of an appropriate intensity normalization of the images prior to the OF application since the local intensity variations would otherwise considerably violate the constant intensity assumption used for the derivation of the brightness transport equation. The error budget for images with properly applied intensity normalization compete with undisturbed reference images. It was shown that the shorter the time difference (Δt) between image pairs, the smaller the error budget calculated, leading to the recommendation that the OF method performs best for small pixel displacements between images.

References

[1] J. L. Barron, D. J. Fleet, and S. S. Beauchemin. Performance of optical flow techniques. *International Journal of Computer Vision*, 12:43–77, 1994. 10.1007/BF01420984.

[2] J. Fokken, R. Kapulla, G. Galgani, O. Schib, K. Pawa, and H. Prasser. Lif-measurements and self-similarity considerations in a stably startified isokinetic turbulent mixing layer. In *Fachtagung "Lasermethoden in der Strömungsmesstechnik", 7. Ű 9. September, Cottbus*, 2010.

[3] J. Fokken, R. Kapulla, S. Kuhn, C. Dyck, and H.-M. Prasser. Stably stratified isokinetic turbulent mixing layers: Comparison of piv-measurements and numerical calculations. In *Fachtagung "Lasermethoden in der Strömungsmesstechnik", 8.–10. September, Erlangen*, 2009.

[4] B. K. Horn and B. G. Schunck. Determining optical flow. *Artificial Intelligence*, 17(1-3):185 – 203, 1981.

[5] B. Jähn. *Digitale Image Processing*. Springer Verlag, 2005.

[6] R. Kapulla, C. Dyck, M. Witte, J. Fokken, and A. Leder. Optical flow and cross correlation techniques for velocity field calculation. In *Fachtagung 'Lasermethoden in der Strömungsmesstechnik', 8. 10. September 2009, Erlangen*, 2008.

[7] LaVision. *DaVis, Imaging Tools, Product-Manual for DaVis 7.2*. LaVision GmbH, Anna-Vandenhoeck-Ring 19, D-37081 Göttingen, 2009.

[8] B. Lecordier and J. Westerweel. The europiv synthetic image generator (sig). In M. Stanislas, J. Westerweel, and J. Kompenhans, editors, *Particle image velocimetry: recent improvements. EUROPIV 2 workshop*. Springer Verlag, 2003.

[9] K. Okamoto, S. Nishio, T. Saga, and T. Kobayashi. Standard images for particle-image velocimetry. *Measurement Science and Technology*, 11(6):685, 2000.

[10] P. Ruhnau, T. Kohlberger, C. Schnörr, and H. Nobach. Variational optical flow estimation for particle image velocimetry. *Experiments in Fluids*, 38:21–32, 2005. 10.1007/s00348-004-0880-5.

Appendix

The intensity normalization sequence consists in the following steps:

1. A sliding minimum filter (SMF) is applied to the image: $I_{smf}(i,j) = SMF\{I(i,j)\}$
2. The difference between the original image and $I_{smf}(i,j)$ is calculated: $I_{diff}(i,j) = I(i,j) - I_{smf}(i,j)$
3. A strict sliding maximum filter (SSMF) is applied to the original image: $I_{ssmf}(i,j) = SSMF\{I(i,j)\}$
4. The ratio between the maximum mapping intensity I_{map} (usually it applies $I_{map} = 1$) and $I_{ssmf}(i,j)$ is calculated: $I_{ra}(i,j) = I_{map}/I_{ssmf}(i,j)$
5. And the resulting normalized image can thus be calculated from: $I_n(i,j) = I_{diff}(i,j) \cdot I_{ra}(i,j)$
6. Finally, gray-scale intensities $I_n(i,j)$ below 0 and above I_{map} are clipped.

For an image $I(i,j)$ with the coordinate origin in the lower left corner, the **sliding minimum filter** calculates a local minimum over a defined scale length l_s in a four step procedure according to the following algorithm:

- For all $j \in [1 \text{ to } m]$ do $I_{\min} = I_{avg}(1,j) = I(1,j)$
  - For all $i \in [2 \text{ to } n]$ do
    - if $I(i,j) > I_{\min} \rightarrow I_{\min} = \frac{l_s/2-1}{l_s/2} I_{\min} + \frac{1}{l_2/2} I(i,j)$
    - else $\rightarrow I_{\min} = I(i,j)$
    - $I_{avg}(i,j) = \frac{l_s-1}{l_s} I_{avg}(i-1,j) + \frac{1}{l_s} I_{\min}$
- For all $j \in [1 \text{ to } n]$ do
  - For all $i \in [(m-1) \text{ to } 1]$ do
    - $I_{avg}(i,j) = \frac{l_s-1}{l_s} I_{avg}(i+1,j) + \frac{1}{l_s} I_{avg}(i,j)$
- For all $i \in [1 \text{ to } m]$ do
  - For all $j \in [2 \text{ to } n]$ do
    - $I_{avg}(i,j) = \frac{l_s-1}{l_s} I_{avg}(i,j-1) + \frac{1}{l_s} I_{avg}(i,j)$
- For all $i \in [1 \text{ to } m]$ do
  - For all $j \in [(n-1) \text{ to } 1]$ do
    - $I_{avg}(i,j) = \frac{l_s-1}{l_s} I_{avg}(i,j+1) + \frac{1}{l_s} I_{avg}(i,j)$

For an image $I(i,j)$, the **strict sliding maximum filter** calculates a local maximum over a defined scale length l_s in a four step procedure according to the following algorithm:

- For all $j \in [1 \text{ to } m]$ do $I_{avg}(1,j) = I(1,j)$
  - For all $i \in [2 \text{ to } n]$ do
    - if $\{I_{avg}(i,j) < I_{avg}(i-1,j)\} \rightarrow I_{avg} = \frac{l_s/2-1}{l_s/2} I_{avg}(i-1,j) + \frac{1}{l_2/2} I(i,j)$
    - else $\rightarrow I_{avg}(i,j) = I(i,j)$
- For all $j \in [1 \text{ to } n]$ do
  - For all $i \in [(m-1) \text{ to } 1]$ do
    - $I_{avg}(i,j) = \max\left\{I_{avg}(i,j),\ \frac{l_s-1}{l_s} I_{avg}(i+1,j) + \frac{1}{l_s} I_{avg}(i,j)\right\}$
- For all $i \in [1 \text{ to } m]$ do
  - For all $j \in [2 \text{ to } n]$ do
    - $I_{avg}(i,j) = \max\left\{I_{avg}(i,j),\ \frac{l_s-1}{l_s} I_{avg}(i,j-1) + \frac{1}{l_s} I_{avg}(i,j)\right\}$
- For all $i \in [1 \text{ to } m]$ do
  - For all $j \in [(n-1) \text{ to } 1]$ do
    - $I_{avg}(i,j) = \max\left\{I_{avg}(i,j),\ \frac{l_s-1}{l_s} I_{avg}(i,j+1) + \frac{1}{l_s} I_{avg}(i,j)\right\}$